Supplementary Materials: Supplement Model: Combining Planar laser-induced fluorescence with stagnation point flows for small single crystal model catalysts: CO oxidation on a Pd(100)

Jianfeng Zhou, Sebastian Matera ,Sebastian Pfaff, Sara Blomberg, Edvin Lundgren and Johan Zetterberg

1. Reactive flow modeling

Our starting point are the governing equations for stationary reactive gas flows in the Low Mach Number Approximation (LMNA)[1]. We neglect the (typically small) Dafour and Soret effects as well as gas phase chemical reactions. The governing partial differential equations then read

$$\nabla \cdot \rho \boldsymbol{v} = 0 \tag{1}$$

$$\nabla \cdot (\rho \boldsymbol{v} \otimes \boldsymbol{v} + p_\mathrm{h} \boldsymbol{I} - \boldsymbol{\tau}) = \rho \boldsymbol{g} \tag{2}$$

$$\rho c_p \boldsymbol{v} \cdot \nabla T - \nabla \cdot \kappa \nabla T + \sum_{i=1}^{N_\mathrm{spec.}} c_{p,i} \boldsymbol{j}_i \cdot \nabla T = 0 \tag{3}$$

$$\rho \boldsymbol{v} \cdot \nabla Y_i + \nabla \cdot \boldsymbol{j}_i = 0 \tag{4}$$

$$\rho = \frac{p_\mathrm{ref.}}{k_\mathrm{B} T \sum_i Y_i / m_i} \tag{5}$$

$$\boldsymbol{\tau} = \mu(\nabla \boldsymbol{v} + \nabla \boldsymbol{v}^T) - \frac{2}{3}\mu \nabla \cdot \boldsymbol{v} \boldsymbol{I} \tag{6}$$

$$\boldsymbol{j}_i = - \sum_{j=1}^{N_\mathrm{spec.}} D_{ij} \nabla Y_j \tag{7}$$

where eqn. 1 to 4 are the mass, momentum, energy and species balance equations, governing the fields of velocity $\boldsymbol{v}$, hydrodynamic pressure p_h, temperature T and mass fractions Y_i of the different gaseous species. Due to the LMNA the mass density ρ is determined by the ideal gas law 5 from the (spatially) constant reference pressure $p_\mathrm{ref.}$ (at the inlet), T, the Boltzmann constant k_B and Y_i (and corresponding molecular masses m_i). The equations are closed by the constitutive relation 6 for the viscous stress $\boldsymbol{\tau}$, with the viscosity μ, and the generalized Fick's law 7 for the diffusive mass fluxes $\boldsymbol{j}_i$, with the diffusion coefficients D_{ij}. The species' heat capacities $c_{p,i}$ can depend on the temperature and by the relation $c_p = \sum_{i=1}^{N_\mathrm{spec.}} c_{p,i} Y_i$ the mixtures heat capacity c_p depends on T and the composition. In general, the transport coefficients μ, λ, D_{ij} and κ (the heat conductivity) depend on ρ, T and Y_i. For the specific formulas for $c_{p,i}$, μ, D_{ij} and κ, we refer to our previous work [2] and references therein.

For the following, we consider Dirichlet boundary conditions (BC) (imposed fields) at the inlet for velocity $\boldsymbol{v}$, temperature T and mass fraction Y_i, where the only restriction is that mass fractions and temperature show no lateral variation on the inlet boundary. For the catalytic surface, we assume non-slip BC for the velocity and that we know the temperature $T_\mathrm{cat.}$. The BC for the mass fractions follow from the species balances for singular surfaces[3]. The BC for the catalytic surface read

$$\boldsymbol{v} = 0, \tag{8}$$

$$T = T_\mathrm{cat.} \tag{9}$$

$$- \sum_{j=1}^{N_\mathrm{spec.}} D_{ij} \boldsymbol{n} \cdot \nabla Y = \nu_i m_i \mathrm{TOF} \tag{10}$$

where we consider only a single overall surface reaction. Here ν_i is the stoichiometric coefficient and TOF is the turnover frequency, which, in the general case, can assume different values at different positions on the catalysts. The normal vector $\boldsymbol{n}$ on the catalytic surface is assumed to point into the gas phase. In the experiment, we measure the temperature $T_{\text{cat.}}$ not at the sample but close to it at the heater. The temperature gradient between the point of measurement and the sample surface has been accounted for by using a calibration created using thermographic phosphors. Hence, we can omit modeling the heat conduction in the solid parts of the setup and instead employ BC 9, with a constant temperature $T_{\text{cat.}}$ for the small samples considered in this study. For remaining solid surfaces, we assume that they are inert and mass balance is obeyed. For the solution of eqn. 1 to 7, detailed BC for temperature and velocity would be needed. However, we target at a reduced model and this detailed information is not important for this.

The first step for the reduced model is to decouple the process of finding the mass fractions from those for the other fields. For this we note, that we are working in large excess of one species. Given the temperature field, the density as well as the thermochemical and transport coefficients will only depend very little on the changes of the mass fractions due to the chemical reactions. Additionally, there is no explicit heat source due to the surface chemical reactions in the governing equations, because we control the temperature of the sample. The equations 1 to 3 will therefor largely decouple from the species balance 4 and, with quite some precision, we can determine ρ, $\boldsymbol{v}$, T and D_{ij} using the solution for zero reactivity (TOF $= 0$). Given this solution, we arrive at the boundary value problem

$$\rho_0 \boldsymbol{v}_0 \cdot \nabla Y_{1,i} - \sum_{j=1}^{N_{\text{spec.}}} \nabla \cdot D_{0,ij} \nabla Y_{1,j} = 0 \tag{11}$$

with the boundary conditions:

$$Y_{1,i} = 0, \quad \text{at the inlet} \tag{12}$$

$$-\sum_{j=1}^{N_{\text{spec.}}} D_{0,ij} \boldsymbol{n} \cdot \nabla Y_{1,j} = \nu_i m_i \text{TOF}, \quad \text{at the catalytic surface} \tag{13}$$

$$\boldsymbol{n} \cdot \nabla Y_{1,i} = 0 \text{ else} \tag{14}$$

where $Y_{1,i} = Y_i - Y_{\text{inl.},i}$ with the mass fraction $Y_{\text{inl.},i}$ at the inlet. The index zero indicates that the respective field, i.e. density, velocity or diffusivity, has be evaluated using the zero reactivity solution. The last BC 14 results from our requirement of inert surfaces (other than the catalyst) and the assumption that we can neglect concentration gradients at the outlet. An alternative way to arrive at the above equations is to perform a formal expansion in the turnover frequency and to truncate after the first order.

For deriving the reduced model, we place the origin of the coordinate system (x, y, z) at the center of the catalyst's surface with the z-axis pointing in the normal direction towards the inlet. A schematic view on the geometry and the flow is shown in figure S1. The PLIF images from the experiment (see main text) reveal that, close to the z-axis, we have concentration variations only along the z-axis. In

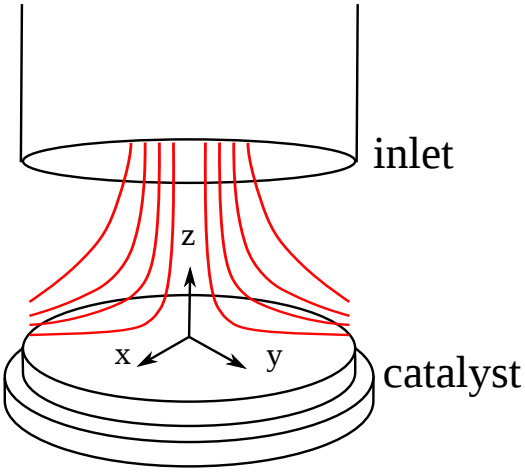

Figure S1. Schematic view of the flow between catalyst and inlet.

other words, first and second derivatives of $Y_{1,j}$ with respect to to x and y vanish in that domain. Thus, we can replace the 3-dimensional problem 11 to 14 with the way simpler problem

$$\rho_0 v_{0,z} \frac{\partial}{\partial z} Y_{1,i} - \sum_{j=1}^{N_{\text{spec.}}} \frac{\partial}{\partial z} D_{0,ij} \frac{\partial}{\partial z} Y_{1,j} = 0 \tag{15}$$

with the boundary conditions:

$$Y_{1,i} = 0, \text{ for } z = L \tag{16}$$

$$\sum_{j=1}^{N_{\text{spec.}}} D_{0,ij} \frac{\partial}{\partial z} Y_{1,j} = -\nu_i m_i \text{TOF}, \quad \text{for } z = 0 \tag{17}$$

where L is the distance between the inlet and the surface. This is now a linear ordinary differential equation boundary value problem with one homogeneous and one inhomogeneous BC. For any two values of the TOF, TOF_a and TOF_b, the respective solutions, $Y_{a1,i}$ and $Y_{b1,i}$, obey the relation

$$\frac{Y_{a1,i}}{Y_{b1,i}} = \frac{\text{TOF}_a}{\text{TOF}_b} \tag{18}$$

at any value of z. If we now have obtained a numerical solution $Y_{\text{ref.},1,i}$ for a reference value $\text{TOF}_{\text{ref.}}$, we can construct the solution for any other value of the TOF by a simple rescaling of our reference solution. Or, if we have a given concentration profile for one species $Y_{\text{given},1,i}$, e.g. from a PLIF measurement, we can estimate the TOF from

$$\text{TOF} = \text{TOF}_{\text{ref.}} \times \frac{\int_0^L Y_{\text{given},1,i} dz}{\int_0^L Y_{\text{ref.},1,i} dz}. \tag{19}$$

Since we have the relation $p_i = Y_i \rho k_B T / m_i$, the same equation holds for the partial pressures p_i. In practice, we choose the limits in the above integrals such that we omit integration over the domain very close to the catalyst and the inlet, because the PLIF signal is biased there.

The above equation 19 is, of course, of only little help, if we do not know $v_{0,z}$ and T_0 (for determining ρ_0 and $D_{0,ij}$). The canonical approach would be to determine these by solving the non-reactive equations numerically for the whole reaction chamber. But, this is a huge computational burden, since due to the combination of PLIF with a flat faced single crystal sample, a highly symmetric setup is impossible and we would need full 3D Computational Fluid Dynamics simulations. Further, this would require the temperature distribution at the reactor walls as BC, which might have a huge impact not only on the temperature field within the chamber but also on the velocity field due

to thermoconvection. Determining the temperature distribution is now a major task as well as the construction of an isothermal chamber, again due to the limitations of the combined single crystal/PLIF approach.

Instead of trying to address the problem with computationally expensive simulations, which additionally carry large uncertainties, we will derive a model which is only valid for the boundary layer above the central part of the catalyst surface. This will then require to fix some parameters and we will use the information in the PLIF signal to determine them. First we notice, that we can, in principle, invert equation 15 to obtain $v_{0,z}$ within the boundary layer, where we have significant concentration gradients, i.e.

$$v_{0,z} = \frac{\sum_{j=1}^{N_{\text{spec.}}} \frac{\partial}{\partial z} D_{0,ij} \frac{\partial}{\partial z} Y_{1,j}}{\rho_0 \frac{\partial}{\partial z} Y_{1,i}}, \quad \text{for } z \in [0, L_{\text{B.}}] \tag{20}$$

given the z-dependent mass fractions and the diffusivities in the layer, where $L_{\text{B.}}$ is the boundary layer thickness. In the isothermal case, $D_{0,ij}$ would be constant and thus $v_{0,z}$ therefore only depends on z just as the mass fractions. In the non-isothermal case, we would expect that the temperature is largely independent of x and y if the mass fractions depend only on z. Then both, T_0 and $v_{0,z}$, only depend on z within the boundary layer and close to the z-axis and, hence, the same holds for ρ and all thermochemical and transport coefficients. From the continuity equation, it further follows that the radial velocity component $v_{0,r}$ depends only linearly on $r = \sqrt{x^2 + y^2}$. Using $v_{0,z} = U(z)$ and $v_{0,r} = rV(z)$, we arrive at the classical stagnation flow equations for the boundary layer[4]

$$\frac{\partial}{\partial z}\rho_0 U - 2\rho_0 V = 0 \tag{21}$$

$$\rho_0 U \frac{\partial V}{\partial z} + \rho_0 V^2 = -\Lambda + \frac{\partial}{\partial z}\mu_0 \frac{\partial V}{\partial z} \tag{22}$$

$$\rho_0 c_{p,0} U \frac{\partial T_0}{\partial z} - \frac{\partial}{\partial z}\kappa_0 \frac{\partial T_0}{\partial z} = 0 \tag{23}$$

$$\frac{\partial \Lambda}{\partial z} = 0 \tag{24}$$

$$\rho_0 = \frac{p_{\text{ref.}}}{k_{\text{B}} T_0 \sum_i Y_{\text{inl.},i}/m_i} \tag{25}$$

$$\rho_0 U \frac{\partial}{\partial z} Y_{1,i} - \sum_{j=1}^{N_{\text{spec.}}} \frac{\partial}{\partial z} D_{0,ij} \frac{\partial}{\partial z} Y_{1,j} = 0 \tag{26}$$

for $z \in [0, L_{\text{B.}}]$ and where the last equation is nothing else than eq. 15. These equations are subject to the BC at the surface:

$$U(z=0) = 0,\ V(z=0) = 0,\ T_0(z=0) = T_{\text{cat.}},\ \left(\sum_{j=1}^{N_{\text{spec.}}} D_{0,ij} \frac{\partial}{\partial z} Y_{1,j}\right)(z=0) = -\nu_i m_i \text{TOF} \tag{27}$$

where the first BC results from mass conservation, and the second is the non-slip BC. At the onset of the boundary layer the BC are:

$$U(z = L_{\text{B.}}) = -U_{\text{B}},\ V(z = L_{\text{B.}}) = V_{\text{B}},\ T_0(z = L_{\text{B.}}) = T_{\text{inl.}},\ Y_{1,i}(z = L_{\text{B.}}) = 0 \tag{28}$$

where the last two represent our knowledge that, at the onset of the boundary layer, we still have only small deviations from the composition and the temperature as at the inlet.

Thus, the problem depends on four parameters: i) the TOF, ii) the boundary layer thickness $L_{\text{B.}}$, and the two velocity boundary values U_{B} and V_{B}. These can now be adjusted to reproduce the experimentally measured concentration profile. We can drop $L_{\text{B.}}$ because the actual thickness

of the boundary layer is determined by the values of U_B and V_B. If we choose $L_{B.}$ too large, this can be compensated by choosing U_B and V_B such that stagnation flow equations and the (optimal) boundary conditions at the true boundary layer onset are still fulfilled. Thus we simply choose $L_{B.} = L$. Furthermore, we can decouple the determination of the TOF from the the estimation of U_B and V_B, since by eq. 18 the normalized mass fractions

$$\tilde{Y}_{1,i} := \frac{Y_{1,i}}{\int_0^L Y_{1,i} dz} \tag{29}$$

are independent of the actual chosen value of the TOF. The same holds for equivalently defined normalized partial pressures. In the first step, we thus calculate the normalized mass fraction (partial pressure) profiles for an arbitrary value of the TOF using eqn. 21 to 28 (with $L_{B.} = L$) and adjust U_B and V_B such that the profiles match the experimentally determined normalized profiles. The value of the TOF and the profiles of the species for which we have no experimental data are then determined according to eqn. 19 and 18, respectively. For the solution of the stagnation flow problem, we employ the same strategy as we have used in ref. [2]. This means the boundary value problem 21-28 is numerically solved using the COLDAE package[5], which uses piecewise polynomial collocation at Gaussian points with adaptive mesh refinement. We choose an initial grid of ten equally sized intervals, a polynomial degree of four and an error tolerance of 10^{-4} for rescaled versions of the dependent variables.

In reality, the PLIF signal has a bias close to the inlet and to the surface and thus the integration limits in eqn. 18, 19 and 29 are chosen such that these regions are left out from the integration. Further, the experimental profile has some background, which we estimate by averaging the signal over the region above the onset of the boundary layer (excluding the part close to the inlet, of course). This we subtract from the original experimental profile because we know that the CO_2 concentration must be (close to) zero there. The integrals over the PLIF signal, required for normalization and estimation of the TOF, have been obtained using the midpoint rule on basis of the pixel width in the PLIF images (i.e. equidistant with a spacing of 0.05 mm). We used the same procedure for integrals over the for the simulation results.

1. Majda, A.; Sethia, J. The Derivation and Numerical Solution of the Equations for Zero Mach Number Combustion. *Comb. Sci. Tech.* **1985**, *42*, 185. doi:10.1080/00102208508960376.
2. Matera, S.; Reuter, K. Transport limitations and bistability for in situ CO oxidation at $RuO_2(110)$: First-principles based multiscale modeling. *Phys. Rev. B* **2010**, *82*, 085446. doi:10.1103/PhysRevB.82.085446.
3. Müller, I. *Thermodynamics*, 1st ed.; Pitman Publishing, Boston, 1985.
4. Kee, R.; Coltrin, M.; Glarborg, P. *Chemically Reacting Flows*; Wiley, Hoboken NJ, 2003.
5. Ascher, U.; Spiteri, R. Collocation Software for Boundary Value Differential-Algebraic Equations. *Siam J. Sci. Comp.* **1994**, *15*, 938. doi:10.1137/0915056.